CHIN. PHYS. LETT. Vol. 37, No. 4 (2020) 044206

Pulse Characteristics of Cavityless Solid-State Laser *

Rui Guo(郭瑞)[1,2], Ye-Wen Jiang(江业文)[1,2], Ting-Hao Liu(刘廷昊)[1,2], Qiang Liu(柳强)[1,2], Ma-Li Gong(巩马理)[1,2,3]**

[1]*Department of Precision Instrument, Tsinghua University, Beijing 100084*
[2]*Key Laboratory of Photon Measurement and Control Technology, Ministry of Education, Tsinghua University, Beijing 100084*
[3]*State Key Laboratory of Tribology, Tsinghua University, Beijing 100084*

(Received 30 December 2019)

We propose a theoretical model (cavityless pulsed solid-state-laser theory) to analyze the pulse characteristics of cavity-less solid-state lasers. A high gain Nd:YVO_4 end-pumped cavityless laser system is adopted to verify the theoretical model. It shows that the performance of output energy and pulse width achieved in cavityless configuration is better than that in resonator configuration when the small-signal gain reaches the saturated level. The simulation results calculated by our theoretical model agree very well with the experimental results. This agreement proves the validity of our theoretical model, which has great importance for theoretical analyses of high gain pulsed laser.

PACS: 42.55.Px, 42.55.Ah, 42.60.Gd, 42.55.Xi DOI: 10.1088/0256-307X/37/4/044206

Although lasers are generally produced in a pair of mirrors which form a cavity configuration, a useful light source can be obtained without such a cavity configuration because weak fluorescent emission can be amplified to amplified spontaneous emission (ASE) under extremely high gain. In this Letter, this kind of light source without cavity configuration is called the cavityless laser. Owing to the continuous spectrum characteristic derived from such a cavityless configuration, cavityless lasers have applications in many fields, such as nonlinear effect suppression[1] and laser guide star.[2,3]

In solid-state lasers, cavityless lasers can realize good spatial characteristics[4,5] and narrow spectral linewidth[6] besides the continuous spectrum characteristic. It has also been proved that short pulses comparable to round-trip time can be generated by high gain solid-state lasers with cavityless configuration. This provides an effective method to produce short nanosecond pulses,[7–9] which can be applied in wide applications such as industrial material processing and laser detection. For such short pulses comparable to round-trip time, traditional rate equations have limitations in analyzing the pulse characteristics described in detail in the following. Therefore, a theoretical model is urgently needed to understand the pulse characteristics of cavityless lasers and provide guidance for design of cavityless lasers.

In this Letter, a theoretical model is established for analyzing the pulse characteristics of cavityless solid-state lasers. By applying laser amplifier theory and accounting for the ASE effect, the limitations in traditional rate equations are avoided when solving the pulse characteristics of cavityless solid-state lasers. A high gain Nd:YVO_4 end-pumped cavityless laser system is adopted to demonstrate the validity of the theoretical model. The pulse characteristics are compared between cavityless configuration and resonator configuration. Numerical simulations are carried out to analyze the pulse characteristics including pulse width, pulse energy, and build-up time by applying the theoretical model. The simulation results match the experimental results very well. This agreement between the numerical simulations and the experimental results proves the validity of our proposed theory.

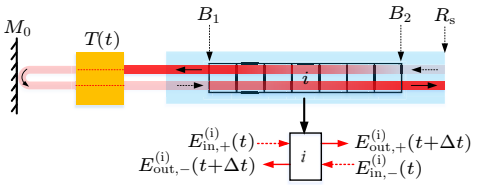

Fig. 1. The configuration of a solid-state cavityless laser.

A simplified configuration of a solid-state cavityless laser is shown in Fig. 1. It consists of a laser gain medium, a high-reflectivity mirror, and a pulsed modulator. Assume that the pumped region is located between B_1 and B_2, and the transmittance function of the pulsed modulator varying with time t is $T(t)$. Ideally, there are no feedbacks in such a cavityless laser without output coupler, but in realistic situations, weak feedback cannot be avoided in such systems due to the very high gain.[4,7] Here we ignore the parasitic feedbacks within the cavityless laser and assume that the effective feedbacks only exist on the right surface of the laser gain medium. The effective reflectivity is referred as R_s in the following text.

In traditional Q-switched rate equation theory, the pulse evolution of a four-level system is described by the equations[10,11]

$$\frac{dn}{dt} = R_p(n_t - n) - \frac{n}{\tau} - W_{up}n^2 - n\sigma_{em}c\phi, \quad (1)$$

$$\frac{d\phi}{dt} = \frac{L_{gain}}{L_{eff}}n\sigma_{em}c\phi - \frac{\phi}{\tau_c}, \quad (2)$$

*Supported by the National Natural Science Foundation of China under Grant No. 62875100
**Corresponding author. Email: gongml@mail.tsinghua.edu.cn
© 2020 Chinese Physical Society and IOP Publishing Ltd

where n is the average inverted population in the gain medium; ϕ is the average photon number density in the cavity; τ, $W_{\rm up}$, $\sigma_{\rm em}$ and $n_{\rm t}$ refers to the fluorescent lifetime, the ETU coefficient, the stimulated emission cross-section and the total doped ions density of the gain medium, respectively. $L_{\rm gain}$ and $L_{\rm eff}$ are the lengths of the gain medium and the optical length within the laser cavity. $R_{\rm p} = \frac{P_{\rm p}}{h\nu_{\rm p}V_{\rm p}n_{\rm t}}$ represents the pump rate, with $P_{\rm p}$ and $V_{\rm p}$ representing the pump power and the pump volume, respectively; h the Planck constant and $\nu_{\rm p}$ the optical frequency of the pump light. Here $\tau_{\rm c}$ is the photon decay time given by

$$\tau_{\rm c} = \frac{t_{\rm r}}{\ln(\frac{1}{R_{\rm OC}}) + L + \delta(t)}, \tag{3}$$

where $t_{\rm r}$ is the round-trip time of the cavity; $R_{\rm OC}$ is the reflectivity of the output coupler; L is the parasitic round-trip loss; and $\delta(t)$ is the loss function determined by Q-switch devices.

There are two limitations in the traditional rate equation theory when solving pulse characteristics of cavityless lasers. Firstly, there is obvious ASE effect in cavityless lasers due to the high gain. The traditional rate equation theory fails to account for the contribution of ASE to the evolution of the pulse. Although there have been some studies on modifying the traditional rate equations by introducing a factor accounting for contribution of spontaneous emission,[12,13] the influence of ASE effect is evaluated by empirically but not theoretically. Secondly, the pulse widths of cavityless lasers are capable of reaching a few number of round-trip time $t_{\rm r}$, which is rarely realized in traditional Q-switched oscillators. The traditional rate equation theory treats the round-trip time as the minimum time unit, which limits the resolution in solving the pulse profile.[11]

To solve the limitations mentioned above, we propose a theoretical model utilizing the laser amplifier theory. Since the calculation of pulse characteristics can be extended to situation of cavityless lasers in solid-state laser, we call this theoretical model the cavity-less-pulse-solid-state-laser theory. The theoretical model consists of three parts: amplification process, boundary condition and initial condition, which will be discussed in the following.

Since the loss is very high in cavityless laser, it requires high small-gain level to realize pulsed output in cavityless laser. There is obvious ASE effect in such cavityless lasers. For the small-signal gain of G_0 along the whole gain region, the intensity of single-pass ASE at the edge of the gain region (B_1 or B_2) can be given by the Linford formula:[14]

$$I_{\rm ASE} = I_{\rm s}\frac{\Omega}{4\pi}\frac{(G_0-1)^{3/2}}{\sqrt{G_0\ln G_0}}, \tag{4}$$

where $I_{\rm s}$ is the saturated intensity and Ω is the solid angle determined by dimensions of the gain region. For the gain region with dimension of $L_{\rm gain}\times W_{\rm gain}\times H_{\rm gain}$ (length, width and height, respectively), $\Omega = W_{\rm gain}H_{\rm gain}/L_{\rm gain}^2$.

The ASE emitted from B_1 will be modulated by the modulator device, and reflected by M_0. A portion of ASE will be reflected back to B_1, enter the gain region and be amplified again. Due to the existence of weak reflectivity of $R_{\rm s}$, a portion of the amplified output at B_2 will be brought back and be amplified again. It can be found that ASE of both the transmitting directions exists within the cavityless laser. Here we define the transmitting direction from B_1 to B_2 as the forward direction, and the inverse direction as the backward direction. To calculate the pulse profile of output laser with high resolution, the gain region is divided into N slices. For an arbitrary gain slice i, there are two terms of seed light and two terms of amplified light. The seed light contains the forward transmitting input and the backward transmitting input, having the flux density of $E^{(i)}_{\rm in,+}$ and $E^{(i)}_{\rm in,-}$, respectively. The flux density of the corresponding amplified light is referred as $E^{(i)}_{\rm out,+}$ and $E^{(i)}_{\rm out,-}$, respectively. The gain of the amplification for the gain slice i (expressed as $G(i)$) can be given by the Frantz–Nodvik formula[15]

$$G^{(i)} = \frac{E_{\rm s}\cdot G_0^{(i)}}{E^{(i)}_{\rm in,+}+E^{(i)}_{\rm in,-}}\ln\left\{1+\left[\exp\left(\frac{E^{(i)}_{\rm in,+}+E^{(i)}_{\rm in,-}}{E_{\rm s}}\right)-1\right]\right\}. \tag{5}$$

Here $E_{\rm s}$ represents the saturated flux density, and $G_0^{(i)}$ is the small-signal gain of the gain slice i. The seed light of two transmitting directions are summed as one seed light to solve the gain $G(i)$. Then the flux density of the amplified output can be further given by

$$\begin{aligned} E^{(i)}_{\rm out,+}(t+\Delta t) &= G^{(i)}(t)\cdot E^{(i)}_{\rm in,+}(t),\\ E^{(i)}_{\rm out,-}(t+\Delta t) &= G^{(i)}(t)\cdot E^{(i)}_{\rm in,-}(t). \end{aligned} \tag{6}$$

The time interval of $\Delta t = L_{\rm gain}/Ncn_{\rm gain}$ is considered between the seed light and the amplified light, where c and $n_{\rm gain}$ are the speed of light in vacuum and the refractive index of the gain medium. In the duration from t to $t+\Delta t$, the variation of inverted population density can be expressed as

$$\begin{aligned} n^{(i)}(t+\Delta t) &= n^{(i)}(t) + R_{\rm p}^{(i)}(t)[n_{\rm t}-n^{(i)}(t)]\Delta t\\ &- \frac{n^{(i)}(t)}{\tau}\Delta t - W_{\rm up}\cdot n^{(i)}(t)^2\cdot\Delta t - A^{(i)}_{\rm ASE}\cdot\Delta t\\ &- \frac{[G^{(i)}(t)-1]\cdot[E^{(i)}_{\rm in,+}(t)+E^{(i)}_{\rm in,-}(t)]}{h\nu\cdot L_{\rm gain}/N}, \end{aligned} \tag{7}$$

where $A^{(i)}_{\rm ASE}$ is the descending rate of inverted population density induced by the single-pass ASE effect. $R_{\rm p}^{(i)}(t)$ is the pump rate for the gain slice i. Assume that the transmitting of the light during the amplification process within the gain region can be treated as plane wave. Once the forward amplified light exits from the ith gain piece, it will further act as the forward direction seed light of the (i+1)th gain piece. The relationship is analogous to the backward amplified light of the ith gain piece and the backward seed light of the (i-1)th gain piece. The relationship can be

expressed as

$$\begin{aligned} E^{(i)}_{\text{out},+}(t) &= E^{(i+1)}_{\text{in},+}(t), \\ E^{(i)}_{\text{out},-}(t) &= E^{(i-1)}_{\text{in},-}(t). \end{aligned} \tag{8}$$

To iterate the relationship (8), the flux density at the boundary of the gain region should be given first, including the flux density of forward seed light at B_1 and backward seed light at B_2, which are referred as $E^{(1)}_{\text{in},+}$ and $E^{(N)}_{\text{in},-}$, respectively. As shown in Fig. 2, the light emits from the edge of the gain region can be divided into two different types considering their different diverging characteristics: (1) the single-pass ASE, which corresponds to the flux density of E_{ASE} and has large divergence angle at B_1/ B_2, (2) the amplified output, which corresponds to the flux density of $E^{(1)}_{\text{in},+}$ or $E^{(N)}_{\text{in},-}$ and can be treated as plane-wave approximately. For the boundary condition of B_1, the seed light of B_1 comes from the light exiting from B_1. After the single-pass ASE and the amplified output exiting from B_1, it would be attenuated due to the diffraction during the round-trip between M_0 and B_1, and experienced twice modulations by the pulsed modulator. Only a portion of light is effectively reflected back by M_0 and injected into B_1 again. Here we only consider the component of plane wave that contributes to the forward seed light. Assume that the components of plane wave for the single-pass ASE and the amplified output are η_{ASE} and η_{out}, respectively. The flux density of the forward seed light at B_1 can be written as

$$\begin{aligned} E^{(1)}_{\text{in},+}\left(t+2\frac{L_{\text{EQ}}+L_{\text{MQ}}}{c}\right) &= T\left(t+\frac{L_{\text{EQ}}}{c}\right) \\ &\cdot T\left(t+\frac{L_{\text{EQ}}+2L_{\text{MQ}}}{c}\right) \\ &\cdot [E_{\text{ASE}}(t)\cdot\eta_{\text{ASE}} + E^{(1)}_{\text{out},-}(t)\cdot\eta_{\text{out}}], \end{aligned} \tag{9}$$

where the time delay during the transmitting is taken into account. L_{EQ} refers to the optical path between B_1 and the modulator; L_{MQ} refers to the optical path between the modulator and M_0. The flux density of the single-pass ASE satisfies $E_{\text{ASE}} = I_{\text{ASE}}\cdot\Delta t$.

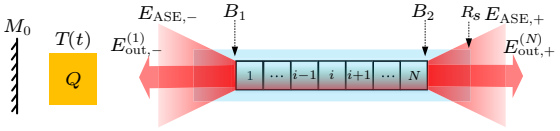

Fig. 2. Diagram of boundary condition in the cavityless laser.

The boundary condition for B_2 is analogous, the backward seed light at B_2 comes from the single-pass ASE and the amplified output reflected by the weak feedback. The flux density of the backward light at B_2 can be expressed as

$$E^{(N)}_{\text{in},-}\left(t+\frac{2L_{\text{ES}}}{c}\right) = R_{\text{s}}[E_{\text{ASE}}(t)\eta_{\text{ASE}} + E^{(N)}_{\text{out},+}(t)\eta_{\text{out}}], \tag{10}$$

where L_{ES} is the optical path between B_2 and the right surface of the gain medium.

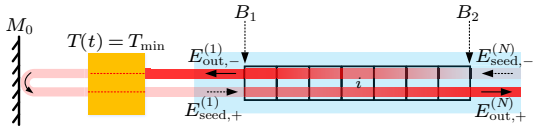

Fig. 3. Diagram of initial condition in cavityless laser.

The initial flux density distribution within the gain region should be given before solving the pulse characteristics by iterating (8). Assume that the inverted population density is uniformly distributed (referred as n_0), and the cavityless laser is operating on steady state at initial time. At this moment, the flux density of the amplified output at an arbitrary position would be invariant after transmitting one round-trip. The steady operating situation is illustrated in Fig. 3. Herein the pulsed modulator is assumed to be high-loss state on initial time, which corresponds to a constant transmittance of $T_{\min}$. The relationship between $E^{(1)}_{\text{in},+}$ and $E^{(1)}_{\text{out},-}$ can be given by applying the boundary condition of B_1:

$$E^{(1)}_{\text{in},+} = T^2_{\min}(E_{\text{ASE}}\eta_{\text{ASE}} + E^{(1)}_{\text{out},-}\eta_{\text{out}}). \tag{11}$$

The relationship between $E^{(N)}_{\text{in},-}$ and $E^{(N)}_{\text{out},+}$ can be also given by applying the boundary condition of B_2:

$$E^{(N)}_{\text{in},-} = R_{\text{s}}(E_{\text{ASE}}\eta_{\text{ASE}} + E^{(N)}_{\text{out},+}\eta_{\text{out}}). \tag{12}$$

Since $T_{\min}$ and R_{s} are small constants, $E^{(1)}_{\text{in},+}$ and $E^{(N)}_{\text{in},-}$ can be treated as small signals, the amplification can be treated as small-signal amplification:

$$\begin{aligned} E^{(N)}_{\text{out},+} &= G_0\cdot E^{(1)}_{\text{in},+}, \\ E^{(1)}_{\text{out},-} &= G_0\cdot E^{(N)}_{\text{in},-}. \end{aligned} \tag{13}$$

Combining (11)–(13), the flux density of amplified output at B_1 or B_2 after one round-trip can be calculated. According to the steady operating assumption, the flux density stays invariant after one round-trip. Based on these expressions, a relationship between the flux density of single-pass ASE and the flux density of the amplified output can be derived,

$$\begin{aligned} E^{(1)}_{\text{out},-} &= \frac{G_0 R_{\text{s}}[1+G_0 T^2_{\min}\eta_{\text{out}}]}{1-G^2_0 T^2_{\min} R_{\text{s}}\eta^2_{\text{out}}}\eta_{\text{ASE}}E_{\text{ASE}}, \\ E^{(N)}_{\text{out},+} &= \frac{1+G_0 R_{\text{s}}\eta_{\text{out}}}{1-G^2_0 T^2_{\min} R_{\text{s}}\eta^2_{\text{out}}}G_0 T^2_{\min}\eta_{\text{ASE}}E_{\text{ASE}}. \end{aligned} \tag{14}$$

Considering the small-signal approximation, the initial flux density within the gain region can be given by

$$\begin{aligned} E^{(i)}_{\text{in},+} &= E^{(N)}_{\text{out},+}\exp\left(-\sigma_{\text{em}}n_0\frac{N-i+1}{N}L_{\text{gain}}\right), \\ E^{(i)}_{\text{in},-} &= E^{(1)}_{\text{out},-}\exp\left(-\sigma_{\text{em}}n_0\frac{i}{N}L_{\text{gain}}\right). \end{aligned} \tag{15}$$

With the initial condition and the boundary condition, the pulsed output characteristics can be solved by utilizing the Frantz–Nodvik amplifier theory. It can be found that the above analyzing process is not limited by the time resolution of round-trip time. Furthermore, the ASE intensity is considered in the analyses of initial condition and boundary condition with

the Linford formula, thus the contribution of ASE to the pulse evolution is also taken into account.

To verify the present theoretical model, a pulsed solid-state laser system with cavityless configuration is established. Since a high small-signal gain condition is required for a cavityless laser, a Nd:YVO_4 end-pumped laser module, which has a compact configuration, is applied in our experiment. In addition, in order to discuss the influence of reflectivity on the output characteristic, control experiments are also implemented for the resonator configuration. Numerical simulations are calculated by utilizing the experimental parameters as the simulation condition. Both experimental results and the simulation results will be discussed in the following.

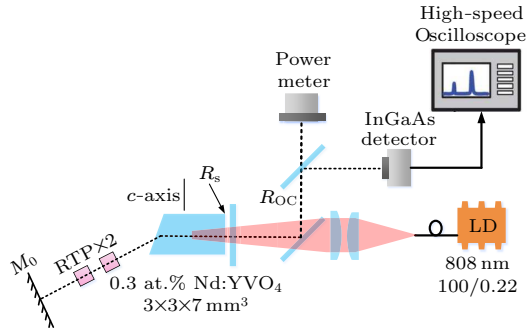

Fig. 4. Experimental setup of high gain Nd:YVO_4 laser system for cavityless and resonator configurations.

The experimental setup is illustrated in Fig. 4. M_0 is the reflector mirror at laser wavelength. A pair of RTP electro-optics crystals are utilized as pulsed modulators for its good performance in high repetition rate. The Nd:YVO_4 crystal with dimensions of $3\times3\times7\,\text{mm}^3$ contains 0.3 at.% dopant. To prevent parasitic oscillations within the crystal, the left end surface of is inclined. The direction of c-axis is parallel to the horizontal plane, as illustrated in Fig. 4. The optical path between M_0 and the right surface of Nd:YVO_4 is ∼55 mm, corresponding to the round-trip time of ∼370 ps. A fiber coupled laser diode (LD) (wavelength of 808 nm, fiber diameter 100 μm and NA = 0.22) is utilized as a pump source. To alleviate the thermal effect in end-pumped lasers, the LD is working on pulsed mode: the repetition rate is 1 kHz, and the duty cycle is 9%, which corresponds to a pump duration of 90 μs. The pump power during the operating duration is 44 W. The beam size is ∼350 μm at the center position of Nd:YVO_4 crystal. Under the high pump density and the pump duration close to the fluorescent lifetime of Nd:YVO_4 (∼95 μs), it can be deduced that the inversion population accumulates to saturated level, and hence obvious ASE emits from both the end surfaces of Nd:YVO_4 crystal. For the cavityless configuration, no output mirror is applied, and there is only effective reflectivity about ∼0.1% residual on the right surface. When a $\lambda/4$ voltage is applied to the electro-optics modulator, ASE with horizontal polarization will be rotated 90° after transmitting a round-trip between M_0 and Nd:YVO_4, and thus the laser operates on high-loss state. While the electro-optics modulator is switched off, the ASE keeps its horizontal polarization invariant and thus corresponds to low-loss state. The pulse build up and extract the gain during the low-loss state. The beam quality factor of the cavityless laser is less than 1.3 on both horizontal and vertical directions. To compare the output pulse characteristics between cavityless configuration and resonator configuration, three control experiments are implemented by placing output mirrors with different reflectivity ($R_{OC} = 10\%$, 20%, 30%, respectively) very close to the right surface of Nd:YVO_4. Once the pulsed laser is output, the output power is measured by a power meter and the pulse profile is observed by a high-speed InGaAs detector (Thorlabs, DET08, bandwidth of 5 GHz) and high speed oscilloscope (Tektronix MSO 73304 DX, sample rate of 100 GS/s, and bandwidth of 33 GHz).

The output characteristics are numerically calculated by applying cavityless pulsed laser theory. The simulation conditions are set to be the experimental parameters. The transmittance function of electro-optics modulator can be written as

$$T(t) = 1 - (1 - T_{\min}) \sin^2 \left(\frac{\pi}{2} \frac{V(t)}{V_{\pi/2}} \right), \qquad (16)$$

where the minimum transmittance $T_{\min}$ is set to be 0.1 and voltage signal $V(t)$ is obtained by experimental measurements. The measured dropping voltage signal $V(t)$ and the corresponding calculated transmittance function $T(t)$ are illustrated in Figs. 5(a) and 5(b). The stimulated emission cross section and the fluorescent lifetime of Nd:YVO_4 is $12\times10^{-19}\,\text{cm}^2$ and 95 μs,[16,17] respectively. The ETU coefficient is $3.2\times10^{-16}\,\text{cm}^2$.[18] The pump region is approximately treated as uniformly distributed. The transmitting efficiency of single-pass ASE (η_{ASE}) is 1.2×10^{-3} and the transmitting efficiency of plane-wave (η_{out}) is set to be 1. The inversion consuming rate induced by single-pass ASE is treated as uniformly distributed within the gain medium, thus it has $A_{\text{ASE}} = \frac{2I_{\text{ASE}}}{h\nu L_{\text{gain}}}$.

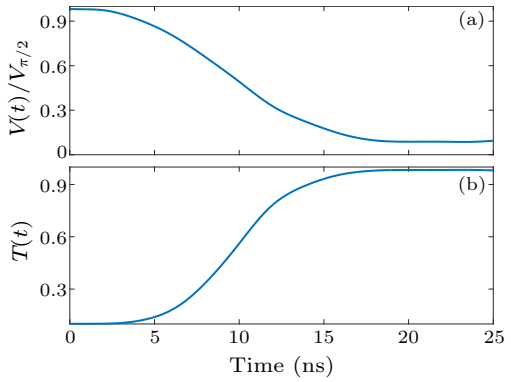

Fig. 5. (a) Measured voltage signal $V(t)$ and (b) the corresponding calculated transmittance $T(t)$.

The pulse width and output energy are illustrated in Figs. 6(a) and 6(b), respectively, for both experimental results and simulation results. The pulse width is defined by the criteria of full width at half

maximum. It can be found that the minimum pulse width and the maximum pulse energy are achieved under cavityless configuration with weak reflectivity. The measured pulse width reaches 550 ps, which is 1.5 times the round-trip duration between M_0 and R_{OC}. The better output performance under cavityless configuration can be attributed to the high saturated small-signal gain and the optimal output coupling condition in this configuration.[10,11] Moreover, it can be found that the simulation results of both pulse width and pulse energy have the same trend with the experimental results, which indicates that the theoretical model is suitable for solving pulse characteristics for both the cavityless configuration with weak-feedback and the resonator configuration with strong feedback.

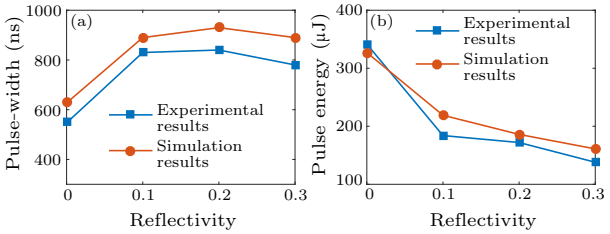

Fig. 6. Comparison between the experimental results and the simulation results of (a) pulse width (b) pulse energy.

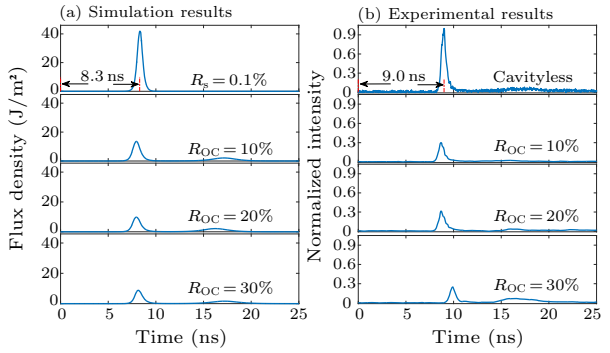

Fig. 7. Pulse waveforms of (a) simulation results and (b) experimental results, under different reflectivity conditions.

The pulse waveforms of different reflectivity for simulation results and experimental results are given in Figs. 7(a) and 7(b), respectively. It is obvious that the pulse amplitude for cavityless weak-feedback configuration is larger than those under the other three reflectivity conditions. The build-up time for different reflectivity has no obvious differences. The simulated build-up time (∼8.3 ns) also matches well to the experimental result (∼9.0 ns), which indicates that the theoretical model can provide good prediction for time-domain pulse characteristic. The good agreement in pulse characteristics between the simulation results and the experimental results proves the validity of the theoretical model we proposed.

In conclusion, we have proposed a theoretical model named as the cavityless pulsed solid-state-laser theory that can analyze the output characteristic of cavityless pulsed solid-state lasers. To test the validity of the theoretical model, an end-pumped Nd:YVO_4 pulsed laser experiment is carried out for observing the output pulse characteristic. By comparing the pulse characteristics between cavityless configuration and resonator configuration, it is shown experimentally that the output of cavityless configuration has narrower pulse width and higher pulse energy than that of resonator configuration under high saturated gain condition. By applying the theoretical model we proposed, numerical simulations are carried out and the results match well with the experimental data. The agreement between the experimental results and the simulations proves the validity of the theory. The cavityless pulsed solid-state-laser theory is of great significance in theoretical analyses of high gain pulsed solid-state lasers.

References

[1] Schmidt O, Wirth C, Rhein S, Rekas M, Kliner A, Schreiber T, Eberhardt R and Tünnermann A 2011 *Advances in Optical Materials* (Istanbul, Turkey 13–16 February 2011) p AMF3
[2] Pique J and Farinotti S 2003 *J. Opt. Soc. Am. B* **20** 2093
[3] Marc F, Guillet de Chatellus H and Pique J 2009 *Opt. Express* **17** 4920
[4] Smith G and Damzen M 2006 *Opt. Express* **14** 3318
[5] Smith G, Damzen M and Shardlow P 2007 *Opt. Lett.* **32** 1911
[6] Chen X, Lu Y, Hu H, Tong L, Zhang L, Yu Y, Wang J, Ren H and Xu L 2018 *Opt. Express* **26** 5602
[7] Young C, Kantorski J and Dixon E 1966 *J. Appl. Phys.* **37** 4319
[8] Guo R, Nie M M, Liu Q and Gong M L 2019 *Opt. Express* **27** 18695
[9] Guo R, Liu Q and Gong M L 2019 *Appl. Opt.* **58** 4701
[10] Degnan J J 1989 *IEEE J. Quantum Electron.* **25** 214
[11] Zayhowski J J and Kelley P L 1991 *IEEE J. Quantum Electron.* **27** 2220
[12] García-López J, Aboites V, Kir'yanov A, Damzen M and Minassian A 2003 *Opt. Commun.* **218** 155
[13] Takashige O, Masahito O, Ara M and Michael D 2006 *Opt. Express* **14** 2727
[14] Svelto O, Taccheo S and Svelto C 1998 *Opt. Commun.* **149** 277
[15] Jeong J, Cho S and Yu T J 2017 *Opt. Express* **25** 3946
[16] Cornacchia F, Turri G, Jenssen H P, Tonelli M and Bass M 2009 *J. Opt. Soc. Am. B* **26** 2084
[17] Guo R, Shen Y J, Meng Y and Gong M L 2019 *Chin. Phys. B* **28** 044204
[18] Cante S, Beecher S J and Mackenzie J I 2018 *Opt. Express* **26** 6478